REVIEW

Stéphane Colin

Rarefaction and compressibility effects on steady and transient gas flows in microchannels

Abstract The main theoretical and experimental results from the literature about steady pressure-driven gas microflows are summarized. Among the different gas flow regimes in microchannels, the slip flow regime is the most frequently encountered. For this reason, the slip flow regime is particularly detailed and the question of appropriate choice of boundary conditions is discussed. It is shown that using second-order boundary conditions allows us to extend the applicability of the slip flow regime to higher Knudsen numbers that are usually relevant to the transition regime.

The review of pulsed flows is also presented, as this kind of flow is frequently encountered in micropumps. The influence of slip on the frequency behavior (pressure gain and phase) of microchannels is illustrated. When subjected to sinusoidal pressure fluctuations, microdiffusers reveal a diode effect which depends on the frequency. This diode effect may be reversed when the depth is shrunk from a few hundred to a few μm.

Thermally driven flows in microchannels are also described. They are particularly interesting for vacuum generation using microsystems without moving parts.

Nomenclature

a	Aspect ratio, h/b (dimensionless)
a_i	Widths of microdiffusers (m)
A_i	Coefficients for second-order slip flow models (dimensionless)
b	Width (m)
c	Mean-square molecular speed (m s^{-1})
d	Molecular diameter (m)
E	Diode efficiency (dimensionless)
Eck	Eckert number (dimensionless)
h	Microchannel depth (m)
k	Boltzmann constant (J K^{-1})
Kn	Knudsen number, $\lambda/2h$ (dimensionless)
L	Characteristic length of the studied volume (m)
L_i	Lengths of diffusers parts (m)
l	Microchannel length (m)
l_{SV}	Characteristic length of a sampling volume (m)
m	Mass of a molecule (kg)
Ma	Mach number (dimensionless)
n	Number density (m^{-3})
$\dot{N}$	Molecular flux (s^{-1})
P	Pressure (Pa)
p	Fluctuating pressure (Pa)
P^*	Pressure gain (dimensionless)
p^*	Fluctuating pressure gain (dimensionless)
Pra	Prandtl number (dimensionless)
q	Mass flow rate (kg s^{-1})
q^*	Reduced mass flow rate, q/q_{NS0} (dimensionless)
r	Specific gas constant (J mol^{-1} K^{-1})
Re	Reynolds number (dimensionless)
Sc	Schmidt number (dimensionless)
T	Temperature (K)
U	Tangential velocity (m s^{-1})
Π	Inlet over outlet pressure ratio, P_i/P_o (dimensionless)

Greek letters

α	Diffuser angle (rad)
δ	Mean molecular spacing (m)
φ	Phase (rad)
γ	Ratio of specific heats (dimensionless)
λ	Mean free path (m)
ρ	Density (m^{3}s^{-1})
σ	Tangential momentum accommodation coefficient (dimensionless)

S. Colin
LGMT—Institut National des Sciences Appliquées,
31077 Toulouse Cedex 4, France
E-mail: stephane.colin@insa-toulouse.fr
Tel.: +33-561-559721
Fax: +33-561-559700

σ_T Thermal accommodation coefficient (dimensionless)

τ Characteristic time of intermolecular collisions (s)

Subscripts
i	Inlet
n	Normal direction
NS0	Navier-Stokes model with no-slip boundary conditions
NS1	Navier-Stokes model with first-order slip flow boundary conditions
NS2	Navier-Stokes model with second order slip flow boundary conditions
QHD1	Quasihydrodynamic model with first-order slip flow boundary conditions
o	Outlet
t	Tangential direction
w	Wall

1 General properties of gas microflows

In microfluidics, knowledge for gas flows is currently more advanced than that for liquid flows. Concerning the gases, the issues are actually more clearly identified: the main microeffect that results from shrinking down the devices size is *rarefaction*. This allows us to exploit the strong—although incomplete—analogy between microflows and low pressure flows, extensively studied for more than fifty years, particularly for aerospace applications.

1.1 Scale effects and rarefaction

Modeling gas microflows requires us to take into account several characteristic length scales. At the molecular level, we may consider the mean molecular diameter, d, the mean molecular spacing, δ, and the mean free path, λ.

Gases that satisfy:

$$\frac{d}{\delta} \ll 1 \tag{1}$$

are said to be *dilute gases*. In this case, most of the intermolecular interactions are binary collisions. Conversely, if Eq. 1 is not verified, the gas is said to be a *dense gas*. The dilute gas approximation, along with the equipartition of energy principle, leads to the classic kinetic theory and the Boltzmann transport equation. For a *simple gas*, composed of identical molecules considered as hard spheres at thermodynamic equilibrium, the mean free path,

$$\lambda = \frac{1}{\sqrt{2}\pi d^2 n} \tag{2}$$

depends on the diameter, d, and the number density $n = \delta^{-3}$ (Bird 1998).

The continuum assumption, when applicable, is very convenient since it erases the molecular discontinuities by averaging the microscopic quantities on a small sampling volume. The continuum approach requires the sampling volume to be in thermodynamic equilibrium. Consequently, the characteristic times of the flow have to be large compared with the characteristic time,

$$\tau = \frac{\lambda}{c} \tag{3}$$

of intermolecular collisions, defined from the mean-square molecular speed:

$$c = \sqrt{3rT} \tag{4}$$

where r is the specific gas constant and T is the temperature. For the thermodynamic equilibrium to be respected, the number of collisions inside the sampling volume must also be high enough. It implies that the mean free path must be small compared with the characteristic length, l_{SV}, of the sampling volume, itself being small compared with the characteristic length L of the studied volume. As a consequence, the thermodynamic equilibrium requires that the Knudsen number satisfy:

$$Kn = \frac{\lambda}{L} \ll 1 \tag{5}$$

Moreover, the Knudsen number, which characterizes the rarefaction of the flow, is related to the Reynolds number, Re, and the Mach number, Ma, by:

$$Kn = \sqrt{\frac{\gamma\pi}{2}}\frac{Ma}{Re} \tag{6}$$

Equation 6 shows the link between rarefaction and compressibility effects, the latter having to be taken into account if $Ma > 0.2$. Finally, the microscopic fluctuations should not generate significant statistical fluctuations of the averaged quantities. It may be considered that sampling a volume that contains 10,000 molecules leads to 1% statistical fluctuations in these quantities. Such a fluctuation level needs a sampling volume such that its characteristic length verifies $l_{SV}/\delta = 10^{4/3} \approx 22$. Consequently, the control volume must have a much higher characteristic length, i.e.,

$$\frac{L}{\delta} \gg 10^{4/3} \tag{7}$$

so that the flow could be precisely modeled with a continuum approach. As an example, for air in standard conditions (i.e., for $T = 273.15$ K and $P = 1.013 \times 10^5$ Pa), $d = 0.37$ nm, $\delta = 3.3$ nm, $\lambda = 65$ nm, $n = 2.7 \times 10^{25}$ m^{-3}, $\tau = 1.34 \times 10^{-10}$ s, and $l_{SV} = 72$ nm is close to the value of the mean free path, λ.

1.2 Flow regimes classification

The limits that correspond to Eqs. 1, 5, and 7, with the indicative values ($\delta/d = 7$, $L/\delta = 100$, and $\lambda/L = 0,1$)

proposed by Bird (1998), are shown in Fig. 1. It is clear that the similitude between low pressure and confined flows is not complete, since the Knudsen number is not the only parameter to take into account.

However, it is convenient to differentiate the flow regimes as a function of Kn, and the following classification, although tinged with empiricism, is usually accepted:

1. For $Kn < 10^{-3}$, the flow is a *continuum flow* (**C**) and it is accurately modeled by the Navier-Stokes equations with classical no-slip boundary conditions
2. For $10^{-3} < Kn < 10^{-1}$, the flow is a *slip flow* (**S**) and the Navier-Stokes equations remain applicable, provided a velocity slip and a temperature jump are taken into account at the walls
3. For $10^{-1} < Kn < 10$, the regime is a *transition* regime (**T**) and the continuum approach of the Navier-Stokes equations is no longer valid. However, the intermolecular collisions are not yet negligible and should be taken into account
4. For $Kn > 10$, the regime is a *free molecular* regime (**M**) and the occurrence of intermolecular collisions is negligible compared with the one of collisions between the gas molecules and the walls
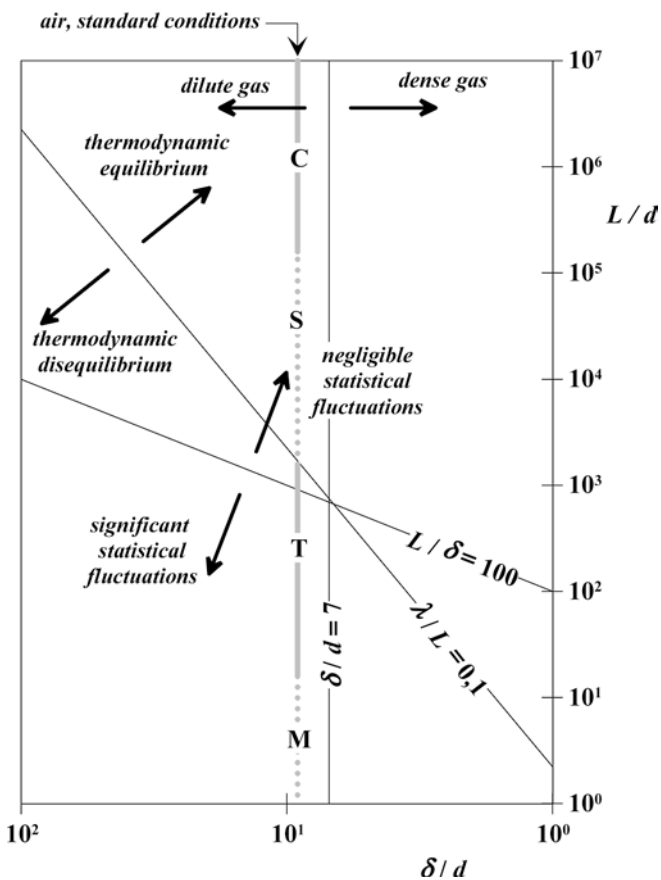
The limits of these different regimes are only indicative and could vary from one case to another, partly because the choice of the characteristic length, L, is rarely unique. In complex geometrical configurations, it is generally preferable to define L from local gradients (for example, the density ρ : $L = 1/|\nabla\rho/\rho|$) rather than from simple geometrical considerations (Gad-el-Hak 1999); the Knudsen number based on this characteristic length is the so-called local *rarefaction number* (Lengrand and Elizarova 2004). Figure 1 locates these different regimes for air in standard conditions, considered as a dilute gas, along a gray vertical line.

The relationship with the characteristic length, L, expressed in μm is illustrated in Fig. 2, which shows the typical ranges covered by fluidic microsystems presented in the literature. Typically, most of the microsystems which use gases work in the slip flow regime, or in the early transition regime. In simple configurations, such flows can be analytically or semi-analytically modeled. The core of the transition regime relates to more specific flows that involve lengths under one hundred μm, as in the case of hard disk drives. In that regime, the only theoretical models are molecular models that require numerical simulations. Finally, under the effect of both low pressures and small dimensions, more rarefied regimes can occur, notably, inside microsystems dedicated to vacuum generation.

2 Pressure-driven steady microflows

2.1 Slip flow regime—analytical models and experiments

Due to its great occurrence in gas microsystems, the slip flow regime has been widely studied, since it leads to quite simple models which further the optimization of these microsystems. The first boundary condition:
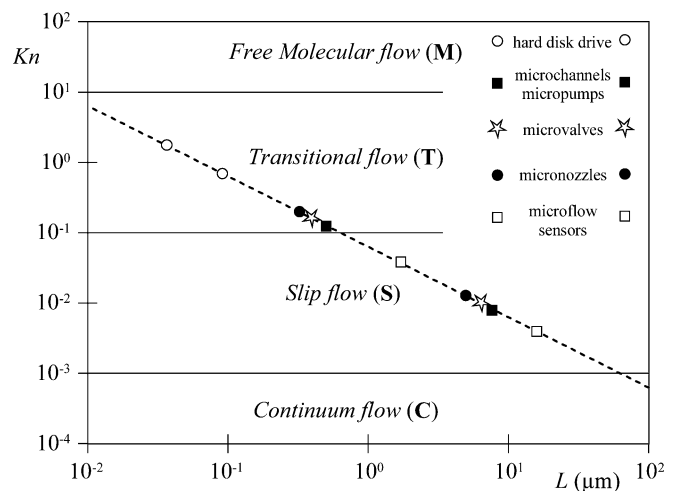

Fig. 1 Limits of the main approximations for the modeling of gas microflows (Bird 1998)

Fig. 2 Characteristic lengths of typical fluidic microsystems, with the range of Knudsen number corresponding to standard conditions (Karniadakis and Beskok 2002)

$$U_t - U_w = \frac{2-\sigma}{\sigma} Kn \frac{\partial U_t}{\partial n} + \frac{3}{2\pi} \frac{\gamma-1}{\gamma} \frac{Kn^2 Re}{Eck} \frac{\partial T}{\partial t} \qquad (8)$$

which expressed a slip of velocity at the wall, was proposed by Maxwell (1879), and that which expressed a jump of temperature:

$$T - T_w = \frac{2-\sigma_T}{\sigma_T} \frac{2\gamma}{\gamma+1} \frac{Kn}{Pra} \frac{\partial T}{\partial n} \qquad (9)$$

was proposed by Smoluchowski (1898). They are written above in a non-dimensional form. The subscript w relates to the wall and the subscripts t and n to the tangential and normal (exiting the wall) directions, respectively. In the gas, at the contact point with the wall, the tangential velocity is denoted as U_t and the temperature as T. The ratio of the specific heats is denoted as γ. The Reynolds Re, the Prandtl Pra, and the Eckert Eck numbers play a role if the flow is not isothermal. Actually, there are only three independent non-dimensional parameters (Pra, Re, and Kn), since

$$Eck = (\gamma - 1) \frac{T_0}{\Delta T} Ma^2 \qquad (10)$$

and

$$Kn = \sqrt{\frac{\gamma\pi}{2}} \frac{Ma}{Re} \qquad (11)$$

The tangential momentum and thermal accommodation coefficients, σ and σ_T, respectively, account for the interactions of the gaseous molecules with the wall. Their precise determination remains problematic, because it depends on the nature of the gas and the wall, as well as on the state of the surface. A purely specular reflection corresponds to $\sigma = 0$, whereas a totally diffuse reflection corresponds to $\sigma = 1$. Likewise, after a collision with the wall, a molecule acquires the temperature of the wall if $\sigma_T = 1$ and keeps its own initial temperature if $\sigma_T = 0$.

The second term in Eq. 8 is responsible for the thermal creep (or transpiration) effect, which can cause a pressure variation and, consequently, the fluid motion (from cold to hot temperatures) in the sole initial presence of tangential temperature gradients. In the absence of this wall tangential gradient ($\partial T/\partial t = 0$), the boundary conditions in Eqs. 8 and 9 are called first-order (i.e., $\vartheta(Kn)$) boundary conditions; the velocity slip (respectively, the temperature jump) is then proportional to the transverse velocity (respectively, the temperature) gradient and to the Knudsen number, Kn.

From a theoretical point of view, the slip flow regime is particularly interesting because it generally leads to analytical or semi-analytical models. These analytical models allow us to calculate velocities and flow rates for isothermal and locally fully developed flows between plane plates or in cylindrical ducts with simple sections: circular (Kennard 1938), annular (Ebert and Sparrow 1965), rectangular (Ebert and Sparrow 1965; Morini and Spiga 1998), etc. These models proved to be quite precise

for moderate Knudsen numbers, typically, up to about 0.1 (Harley et al. 1995; Liu et al. 1995; Shih et al. 1996; Arkilic et al. 2001).

For $Kn > 0.1$, experimental studies (Sreekanth 1969) or numerical studies (Piekos and Breuer 1996) with the direct simulation Monte Carlo (DSMC) method show significant deviations with models based on first-order boundary conditions. Since 1947, several authors have proposed second-order boundary conditions, hoping to extend the validity of the slip flow regime to higher Knudsen numbers. Second-order boundary conditions take more or less complicated forms, which are difficult to group together in a sole equation. Actually, according to the assumptions, the second-order terms ($\vartheta(Kn^2)$) may be dependent on σ (Chapman and Cowling 1952; Karniadakis and Beskok 2002) and may involve tangential second derivatives $\partial^2 U/\partial t^2 = 0$ (Deissler 1964). In the simple case of a developed flow between plane plates, the tangential second derivatives are zero, and one may compare most of the second-order models which take the generic form:

$$U_t - U_w = A_1 Kn \frac{\partial U_t}{\partial n} + A_2 Kn^2 \frac{\partial^2 U_t}{\partial n^2} \qquad (12)$$

In the particular case of a fully diffuse reflection ($\sigma = 1$), the coefficients A_1 and A_2 proposed in the literature are compared in Table 1.

We note significant differences, essentially for the second-order term. Moreover, some models based on a simple mathematical extension of Maxwell's condition predict a decrease of the slip compared to the first-order model, while other models predict an increase of the slip.

The latter, based on a physical approach of the behavior of the gas near the wall, follow the same trend of some recent experimental observations. Lalonde (2001) measured the rate of helium and nitrogen flows in microchannels and showed that, for outlet Knudsen numbers Kn_o higher than 0.05, a first-order model underestimates the slip. A second-order model (Aubert and Colin 2001) based on the boundary conditions of Deissler (1964) was in very good agreement with the experimental data up to $Kn_o \approx 0.25$, with an accommodation coefficient of $\sigma = 0.93$ both for helium and

Table 1 Coefficients of the main models of second-order boundary conditions proposed in the literature

Source	A_1	A_2
Maxwell (1879)	1	0
Schamberg 1947 (Karniadakis and Beskok 2002)	1	$-5\pi/12$
Chapman and Cowling (1952)	κ_0 (≈ 1)	$\kappa_0^2/2$ ($\approx 1/2$)
Cercignani 1963 (Karniadakis and Beskok 2002)	1.1466	-0.9756
Deissler (1964)	1	$-9/8$
Hsia and Domoto 1983 (Karniadakis and Beskok 2002)	1	-0.5
Mitsuya (1993)	1	$-2/9$
Karniadakis and Beskok (2002)	1	$1/2$

nitrogen (Colin et al. 2004). Figure 3 shows the comparison between experimental and theoretical data relative to the reduced flow rate $q^* = q/q_{NS0}$ for an inlet over outlet pressure ratio of $\Pi = 1.8$.

This trend was confirmed later by Maurer et al. (2003). The latest precise experimental data provided in the literature (Table 2) follow the same trend; they concern different gases and are relative to microchannels with rectangular sections of comparable lengths, l, and depths, h, but manufactured with different processes. Arkilic et al. (2001) used two silicon wafers facing each other, Colin et al. (2004) studied microchannels etched by deep reactive ion etching (DRIE) in silicon and covered with a glass sealed by anodic bonding, whereas Maurer et al. (2003) used microchannels etched in glass and covered with silicon.

A smart comparison of the data provided by these authors is also tricky, since the aspect ratio, a (ratio of the depth, h, over the width, b), of the sections are different from one study to another. Moreover, if a is larger than 1%, the effects of the lateral walls are no longer negligible, and the plane flow model should be dropped and replaced by a model appropriate to rectangular sections (Aubert and Colin 2001). The two latter studies (Maurer et al. 2003; Colin et al. 2004) confirm that an adequate slip flow model based on second-order boundary conditions can be precise for high Knudsen number that usually come under the transition regime. It should be noted that the resolution of the Navier-Stokes equations with the second-order boundary conditions summarized in Table 1 may turn out to be problematic with some geometrical configurations, searching both numerical and analytical solutions.

Actually, the Navier-Stokes equations correspond to an approximation of the Boltzmann equation, which is first-order in Knudsen ($\vartheta(Kn)$), and should be, strictly speaking, associated only with first-order boundary conditions (Karniadakis and Beskok 2002). The obvious interest in using high-order boundary conditions led some authors to propose new conditions which fit the Navier-Stokes equations better. Thus, Beskok and Kardianakis (1999) put forward a high-order form,

Fig. 3 Inverse reduced flow rate $(1/q^*)$ in rectangular microchannels. Comparison of experimental data with first-order (NS1) and second-order (NS2) slip flow models. $\Pi = 1.8$; $T = 294.2$ K. Gas: N_2 (circles) and He (squares). Microchannel 1 (white): $h = 1.88$ μm; $a = 0.087$. Microchannel 2 (gray): $h = 1.16$ μm; $a = 0.055$. Microchannel 3 (black): $h = 0.54$ μm; $a = 0.011$
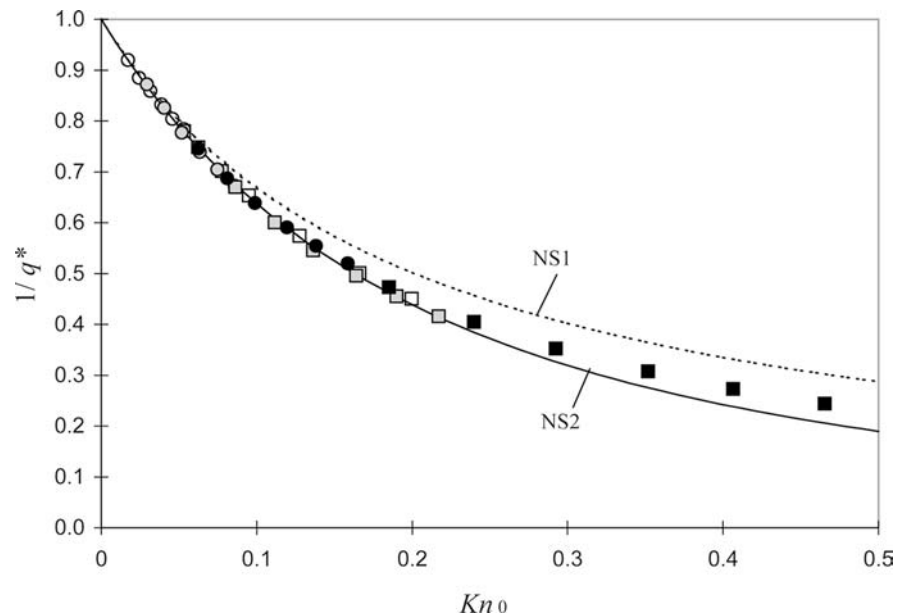
Table 2 Recent experimental data of gas flows in rectangular microchannels

Reference		Arkilic et al. (2001)			Colin et al. (2004)		Maurer et al. (2003)	
Microchannel dimensions	l (μm)	7,490			5,000		10,000	
	h (μm)	1.33			0.54–4.48		1.14	
	a (%)	2.5			1.1–8.7		0.6	
Experimental conditions	Gas	Ar	N_2	CO_2	N_2	He	N_2	He
	Kn_o	0.05–0.41	0.05–0.34	0.03–0.44	0.002–0.16	0.029–0.47	0.054–01.1	0.17–1.46
Theoretical comparison	σ	0.80	0.80	0.80	0.93	0.93	0.87	0.91
	Model	Plane, first-order			Rectangular, second-order $A_2 = -9/8$ (Deissler conditions)		Plane, second-order $A_2 = -0.23_{(N2)}$, $A_2 = -0.26_{(He)}$	

$$U_{\mathrm{t}} - U_w = \frac{2-\sigma}{\sigma} \frac{Kn}{1-cKn} \frac{\partial U_{\mathrm{t}}}{\partial n} \qquad (13)$$

that involves the sole first derivative of the velocity and an empirical parameter c. As for Xue and Fan (2000), they proposed:

$$U_{\mathrm{t}} - U_w = \frac{2-\sigma}{\sigma} \tanh{(Kn)} \frac{\partial U_{\mathrm{t}}}{\partial n} \qquad (14)$$

that leads to results close to that calculated by the DSMC method, up to high Knudsen numbers, of the order of 3. Other hybrid boundary conditions, such as (Jie et al. 2000):

$$U_{\mathrm{t}} - U_w = \frac{2-\sigma}{\sigma} \left[Kn \frac{\partial U_{\mathrm{t}}}{\partial n} + \frac{Kn}{2} \left(Re \frac{\partial P}{\partial t} \right) \right] \qquad (15)$$

were also proposed in order to allow a more stable numerical solution, while giving results comparable to that from Eq. 14 for the cases that were tested.

Lastly, it is also possible to keep the boundary condition of Maxwell, and to replace the Navier-Stokes (NS) equations by the quasihydrodynamic (QHD) equations (Elizavora and Sheretov 2001). The latter differ from the Navier-Stokes equations by a small parameter which introduces some corrections on the flow rate, second-order in Knudsen ($\vartheta(Kn^2)$) (Elizarova and Sheretov 2003). The QHD model with first-order boundary conditions (QHD1) predicts flow rates close to those calculated with the NS model with Deissler second-order boundary conditions (NS2) (Colin et al. 2003). For example, for a flow between parallel plates with an inlet over outlet pressure ratio of Π, the dimensionless mass flow rates:

$$q^*_{\mathrm{QHD1}} = 1 + 12 \frac{2-\sigma}{\sigma} \frac{Kn_{\mathrm{o}}}{\Pi+1} + \frac{48}{\pi Sc} Kn_{\mathrm{o}}^2 \frac{\ln \Pi}{\Pi^2 - 1} \qquad (16)$$

and:

$$q^*_{\mathrm{NS2}} = 1 + 12 \frac{2-\sigma}{\sigma} \frac{Kn_{\mathrm{o}}}{\Pi+1} + 27 Kn_{\mathrm{o}}^2 \frac{\ln \Pi}{\Pi^2 - 1} \qquad (17)$$

only differ by the coefficient of the second-order term ($\vartheta(Kn^2)$).

In Eqs. 16 and 17, the mass flow rates, q, are non-dimensionalized by the mass flow rate, q_{NS0}, of a non-rarefied flow ($q^* = q/q_{\mathrm{NS0}}$). Since the Schmidt number, Sc, is 0.77 for a monatomic gas and 0.74 for a diatomic gas, the deviation between the last terms of Eqs. 16 and 17 is of the order of 25%.

Thus, as the Knudsen number increases, the deviation between the QDH1 and NS2 models increases. For outlet Knudsen numbers, Kn_{o}, higher than 0.1, the experimental data of Lalonde (2001) fit the QHD1 model (Elizavora and Sheretov2001) better than the NS2 model (Aubert and Colin 2001), but with a higher value of the accommodation coefficient: $\sigma_{\mathrm{QHD1}} = 1$, whereas $\sigma_{\mathrm{NS2}} = 0.93$ (Fig. 4).

2.2 Transition regime—numerical simulation

The methods used for the numerical simulation of gaseous microflows depend on the rarefaction level of the flow. So, as long as the regime is a continuum regime ($Kn < 10^{-3}$), a classic simulation (finite difference, finite volume, spectral element, etc.) of the Navier-Stokes equations is appropriate, whatever the characteristic lengths of the domain.

In the slip flow regime, roughly for $10^{-3} < Kn < 10^{-1}$, the continuum approach remains valid, provided slip boundary conditions are properly taken into account. Karniadakis and Beskok (2002) developed the μ Flow code, which resolves the Navier-Stokes equations by the spectral element method. In its compressible version, this code is able to treat 2-D or axi-symmetric subsonic or shock-free transonic flows with high-order slip velocity and temperature jump conditions at the wall.

As the rarefaction increases, typically for $Kn > 10^{-1}$, a molecular approach is required. The direct numerical resolution of the Boltzmann equation,

$$\frac{\partial f}{\partial t} + \mathbf{v} \cdot \frac{\partial f}{\partial \mathbf{x}} + \mathbf{F} \cdot \frac{\partial f}{\partial \mathbf{v}} = Q(f, f^*) \qquad (18)$$

is complex in most cases, and, thus, remains reserved for problems with a quite simple geometry, or when simplifying hypotheses may be assumed. This is the case in the free molecular regime, for which molecular collisions can be neglected. It is also the case when $Kn \to 0$: the method of moments proposed by Grad (1949) or the Chapman–Enskog method (Chapman and Cowling 1952) allows us then to semi-analytically solve the Boltzmann equation.

On the other hand, in the transition regime, its numerical resolution is only possible with approximate methods based on the simplification of the integral term, $Q(f, f^*)$, which describes the intermolecular collisions. Sharipov and Seleznev (1998) provided a description of the different available methods—the BGK equation (Bhatnagar et al. 1954), linearized Boltzmann equation (Cercignani et al. 1994), etc.—with their conditions of validity.

Actually, the so-called molecular methods are better suited to the simulation of the transition regime, which is the case of the DSMC method developed by Bird (1998). Initially extensively used for the simulation of low-pressure rarefied flows (Bird 1978; Muntz 1989), it is now widely used in microfluidics (Stefanov and Cercignani 1994; Piekos and Breuer 1996; Mavriplis et al. 1997; Chen et al. 1998; Oran et al. 1998; Hudson and Bartel 1999; Pan et al. 1999; Wu and Tseng 2001).

The statistical error tied to the DSMC method becomes tricky when the macroscopic velocities are low. Some modifications were proposed to overcome this issue, leading to the DSMC-IP (Fan and Shen1999) or the MB-DSMC (Pan et al. 2001) methods. Moreover, some hybrid DSMC/Navier-Stokes methods allow the simulation of microflows which involve different regimes

Fig. 4a, b Experimental data from Lalonde (2001) (outlet flow rate □ and inlet flow rate ◆), compared to NS2 and QHD1 models. Microchannel 3: $P_o = 75$ kPa, $T = 294.2$ K. **a** Gas: N_2; $\eta = 17.8 \times 10^{-6}$ Pa s; $r = 2.962 \times 10^2$ J kg^{-1}K^{-1}; $Sc = 0.74$. The *encircled* data correspond to $Kn_o = 0.15$. **b** Gas: He; $\eta = 19.6 \times 10^{-6}$ Pa s; $r = 2.079 \times 10^3$ J kg^{-1}K^{-1}; $Sc = 0.77$. The *encircled* data correspond to $Kn_o = 0.47$
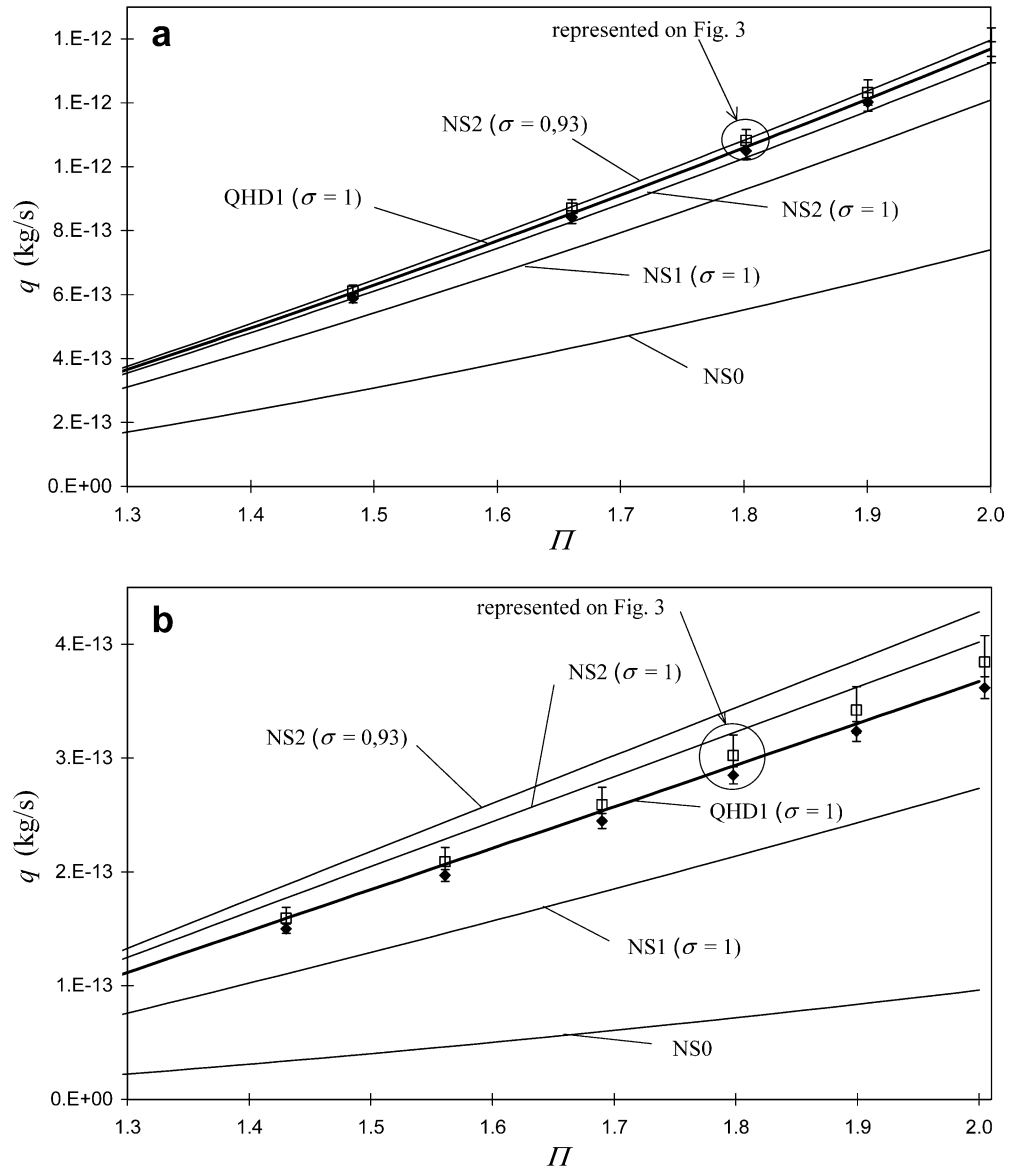
(Hash and Hassan 1997; Roveda et al. 1998). It seems that this kind of issue could be treated by the lattice Boltzmann method. This method is detailed by Chen and Doolen (1998), but its application to microflows remains rare to date.

3 Pressure-driven unsteady microflows

In the literature, little work is reported on unsteady microflows, even in the slip flow regime. Norberg et al. (1997) have experimentally studied transient flows in microchannels with a mass spectrometric system, but for very low transients (of the order of 10 s) and in the molecular regime. Bestman et al. (1995) have considered the Rayleigh problem for slip flow. Arkilic and Breuer (1993) have modeled an unsteady microflow induced by oscillating plates. But since their primary interest was the study of viscous losses due to the oscillating surface, the governing equation only represented a balance between the unsteady and viscous forces. More recently, Caen et al. (1996) presented a model of a pulsed slip flow in microtubes with circular cross-section.

The case of pulsed microflows in rectangular microchannels was modeled by the Navier-Stokes equations combined with first-order slip and temperature jump conditions at the walls (Colin et al. 1998b). The inlet of the microchannel was submitted to a sinusoidal pressure fluctuation with a small amplitude. The gain of the microchannel, i.e., the ratio of the outlet over inlet fluctuating pressure amplitudes, was calculated. For example, in the simple case of a microchannel closed at its outlet, the gain takes the form:

$$p^* = \left| \frac{\Delta p_o}{\Delta p_i} \right| = \left| \frac{1}{\cosh(\beta l)} \right| \tag{19}$$

where $\beta(f, Kn) \approx \sqrt{f}\Psi(Kn)$ depends on the frequency, f, and the Knudsen number. It was shown that the band pass of the microchannel was underestimated when slip at the walls was not taken into account (Fig. 5).

Obtaining experimental data to discuss these theoretical results is very hard, due to the very small size of the pressure sensors required for these experiments. However, first experimental data were obtained for microtubes down to 50 μm in diameter using a commercially available pressure microsensor placed in a minichannel, connected in series to one or several parallel microtubes (Colin et al. 1998a). The behavior of the micro- and minichannels association was simulated and compared to these data (Fig. 6). The agreement was good, both for the gain and the phase of the association.

The previous model was extended to slowly varying cross-sections (Aubert et al. 1998), in order to understand the behavior of microdiffusers subjected to sinusoidal pressure fluctuations. This model was also used to test the diode effect of a microdiffuser/nozzle placed in a microchannel and subjected to sinusoidal pressure fluctuations at its inlet. Two layouts (A and B) were considered (Fig. 7).

In layout A, the tested element was a diffuser, with an increasing section from inlet to outlet. In layout B, the same element was used as a nozzle, with a decreasing section from inlet to outlet. To obtain an exploitable comparison between the two layouts, the dimensions $(a_1, a_2, a_3, L_1, L_2, L_3)$ were the same in both.

The analysis of the frequency behavior for each layout showed significant differences, which is characteristic of a dynamic diode effect. Therefore, in order to characterize the dissymmetry of the pressure fluctuations transmission, an efficiency, E, of the diode was introduced. This efficiency,

$$E = \frac{P_A^*}{P_B^*} = \frac{|\Delta p_o/p_i|_A}{|\Delta p_o/p_i|_B} \qquad (20)$$
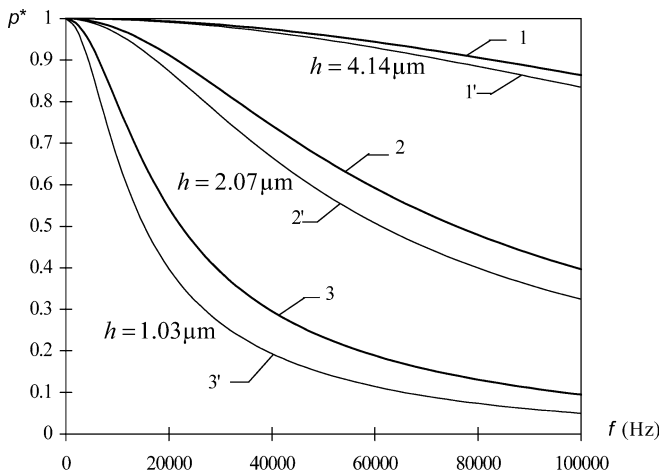
defined as the ratio of the fluctuating pressure gain in layout A over the fluctuating pressure gain in layout B, was studied as a function of the frequency. Some results are shown in Fig. 8 for different values of the depth, h, with $L_1 = L_2 = L_3 = 3$ mm, $a_1 = a_3 = 467$ μm, and $a_2 = 100$ μm, which corresponds to an angle $\alpha = 3.5°$.

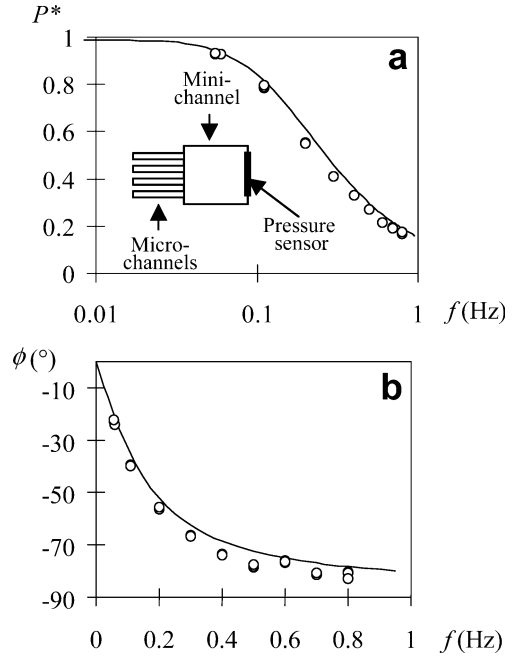The main result was: with a microdiffuser ($h = 6$ μm), E appears to be less than unity *below* a critical

Fig. 6 Experimental gain and phase compared to theory. Four microtubes ($d = 52.5$ μm, $l = 30.2$ mm) in parallel connected to a minitube ($D = 2.5$ mm, $L = 30.5$ mm) with a pressure sensor at its closed end. **a** Gain. **b** Phase of the association

Fig. 5 Influence of microchannel depth, h, on the gain, p^*, for a square microchannel closed at its outlet. $l = 100$ μm, $T = 293$ K, $P = 0.11$ MPa. *1, 2, 3* = slip flow; *1′, 2′, 3′* = no-slip flow
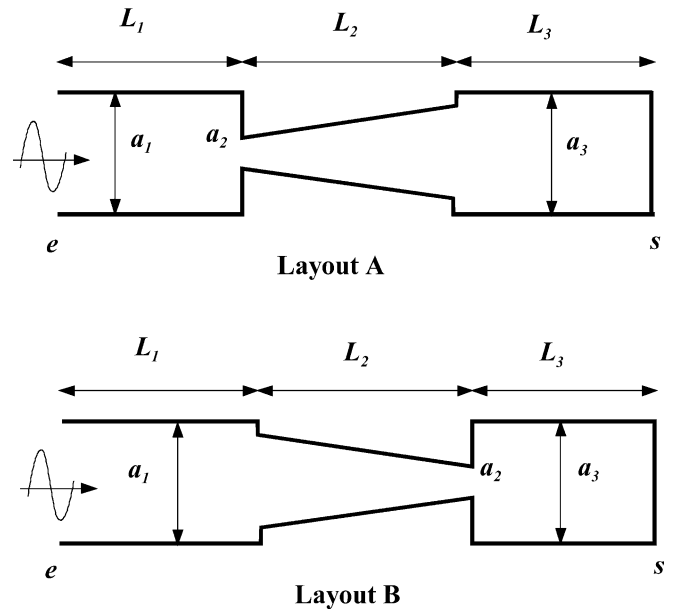

Fig. 7 Two layouts of a microdiode placed in a microchannel
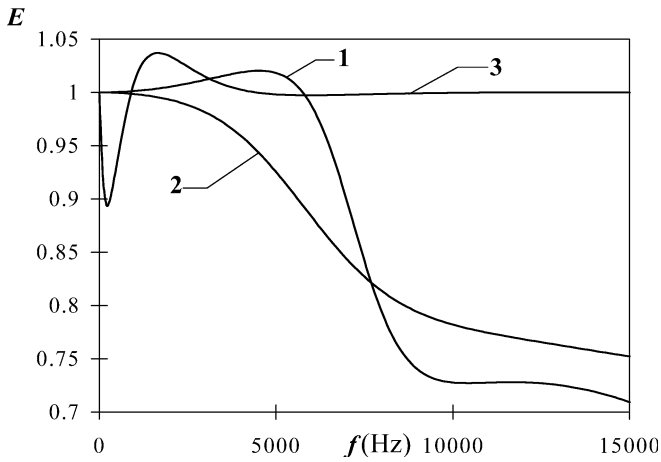
Fig. 8 Diode efficiency for different values of the depth. *1*: $h = 100$ μm; *2*: $h = 62$ μm, *3*: $h = 6$ μm

frequency. This denotes a reversed diode effect compared with the case of a diffuser with millimetric or submillimetric dimensions ($h = 100$ μm in Fig. 8), for which E is less than unity *beyond* a critical frequency. Note also that the influence of slip (taken into account in Fig. 8) is not negligible when $h = 6$ μm. However, slip has little influence on the values of characteristic frequencies (i.e., the frequencies for which E is an extremum or equal to unity).

4 Thermally-driven flows and vacuum generation

Generating vacuum by means of microsystems concerns various applications, such as the taking of biological or chemical samples, and the control of the vacuum level in the neighborhood of some microsystems during their manufacturing or their working.

The properties of rarefied flows allow unusual pumping techniques. For high Knudsen numbers, the flow may be generated without any moving mechanical components, but only using a thermal actuation, which is not possible with classical macropumps.

4.1 Thermal transpiration pumping

Currently, the most studied technique is based on thermal transpiration. The basic principle requires two chambers filled with gas and linked with an orifice whose hydraulic diameter is small compared with the mean free path of the molecules. Chamber 1 is heated, for example, with an element, so that $T_1 > T_2$. By analyzing the probability that some molecules issuing from one chamber cross the orifice, it can be shown that, if the pressure is uniform ($P_1 = P_2 = P$), a molecular flux,

$$\dot{N}_{2\rightarrow 1} = A\sqrt{2\pi mk}P\frac{\sqrt{T_1} - \sqrt{T_2}}{\sqrt{T_1 T_2}} \qquad (21)$$

from chamber 2 towards chamber 1—from cold to hot temperatures—appears (Muntz and Vargo 2002; Lengrand and Elizarova2004), and, if the net molecular flux is constant, the pressures necessarily verify:

$$\frac{P_1}{P_2} = \sqrt{\frac{T_1}{T_2}} \qquad (22)$$

In Eqs. 21 and 22, m is the mass of a molecule and k is the Boltzmann constant. If $P_21_2\sqrt{T_1/T_2}$, there is a net flow from 2 towards 1, which results in a decrease of P_2 and/or an increase of P_1: a basic working microscale pump.

Thus, a Knudsen compressor (Fig. 9) can be designed, connecting a series of chambers with very small orifices which have a cold region (temperature T_2) on one side and a hot region (temperature T_1) on the other side by means of an adequate local heater placed just downstream of the orifices. This multistage layout leads to important cumulated pressure drops, whilst keeping a satisfactory flow rate. In practice, the orifices must be replaced by microchannels (Fig. 9) and this complicates the modeling (Vargo and Muntz 1996). Moreover, it is generally difficult to maintain simultaneously a free molecular regime in the microchannels and a continuum regime in the chambers, which are the conditions required for the optimal efficiency corresponding to Eqs. 21 and 22. More elaborate models, based on the linearization of the Boltzmann equation (Loyalka and Hamoodi 1990) are able to take into account the transition regime ($0.05 < Kn < 10$), both in the microchannels and in the chambers (Vargo and Muntz 1999). Several design studies are proposed in the literature; they show the theoretical feasibility of microscale thermal transpiration pumps.
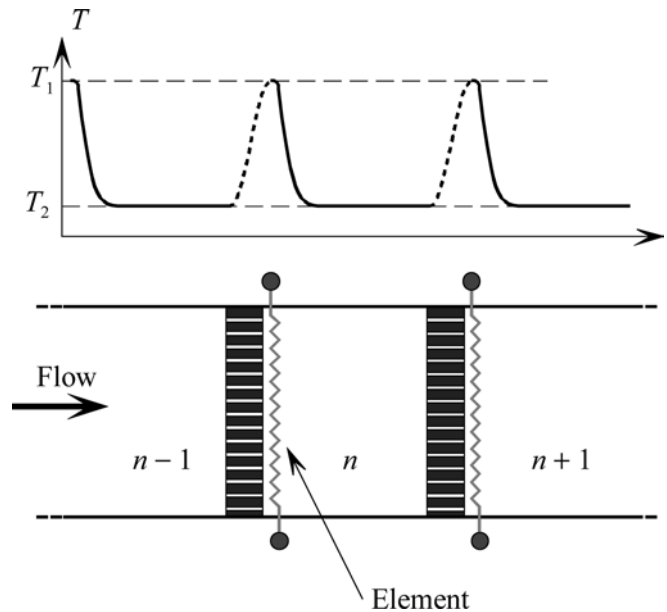

Fig. 9 Multistage Knudsen compressor

The first mesoscale prototypes, heated with an element at the wall (Vargo and Muntz 1997; Vargo and Muntz 1999; Vargo et al. 1999), were tested. An alternative solution with heating within the gas was also proposed (Young 1999), but there are no available experimental data for this layout.

Actually, there is yet much to do for the theoretical optimization and almost everything is to be done for the design of thermal transpiration micropumps with micromanufacturing techniques. The performances of these micropumps remain limited for technological reasons. A high vacuum level may become incompatible with the typical internal sizes of microsystems (Muntz and Vargo 2002): the regime in the chambers must be close to a continuum regime, which requires sizes too big for the lower pressures.

4.2 Accommodation pumping

The accommodation pumping is another pumping technique. It exploits the property of gas molecules whose reflection on specular walls depends on their temperature. If the wall is warmer than the gas, the mean reflection angle is greater than the incident angle. Conversely, if the wall is colder than the molecules, they have a more tangential reflection. Consequently, in a microchannel with perfectly specular walls connecting two chambers at different temperatures, a flow takes place from the hot towards the cold chambers (Hobson 1970). If the walls of the microchannel give a diffuse reflection, this effect disappears. This property was confirmed with numerical simulations by the DSMC method (Hudson and Bartel 1999). Linking two warm chambers (1 and 3) to a cold chamber (2) on one side with a smooth microchannel (1–2) and on the other side with a rough microchannel (3–2), a difference of pressure appears between the two chambers having the same temperature (Fig. 10).
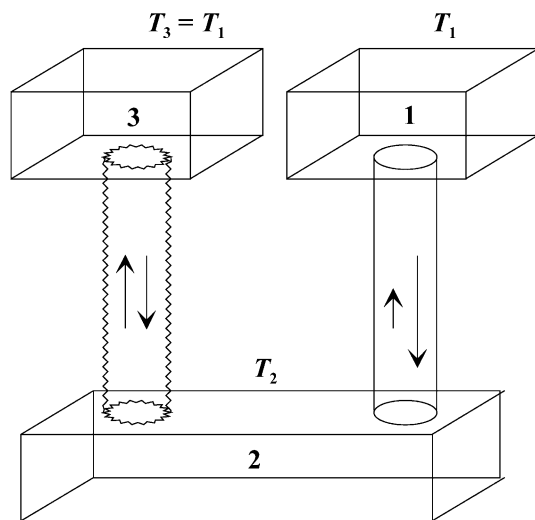
Connecting in series several stages of that type, the pressure drops relative to each stage can be cumulated and this allows to reach high vacuum levels. The advantage of the accommodation pump is that it is operational without theoretical limitations concerning low pressures: contrary to the thermal transpiration pumping, the accommodation pumping does not require chambers with high dimensions. In compensation, the accommodation pump requires more stages to reach the same final pressure ratio. A pressure ratio, $\Pi = 100$, requires 125 stages, whereas only 10 stages are enough for a transpiration pump with comparable temperatures. Lastly, although the concept seems attractive, no operational prototype was described in the literature so far. The most high-performance design was proposed by Hobson (1971; 1972); it requires a cold temperature, $T_2 = 77$ K, for an atmospheric temperature, $T_1 = T_3 = 290$ K.

5 Remaining issues

Theoretical knowledge is currently more advanced for gas flows than for liquid flows in microchannels. However, there is yet a need for precise experimental data, both for steady or unsteady gas microflows, in order to definitely validate the choice of the best boundary conditions in the slip flow regime. Determining the appropriate values of the accommodation coefficients also remains an open issue. Relationships between these values, the nature of the substrate, and the microfabrication processes involved are currently not available. Theoretical investigations relative to unsteady or thermally-driven microflows would also need to be supported by smart experiments.

Fig. 10 One stage of an accommodation micropump

References

Arkilic EB, Breuer KS (1993) Gaseous flow in small channels. AIAA paper, 93–3270, pp 1–7
Arkilic EB, Breuer KS, Schmidt MA (2001) Mass flow and tangential momentum accommodation in silicon micromachined channels. J Fluid Mech 437:29–43
Aubert C, Colin S (2001) High-order boundary conditions for gaseous flows in rectangular microchannels. Microscale Therm Eng 5(1):41–54
Aubert C, Colin S, Caen R (1998) Unsteady gaseous flows in tapered microchannels. In: Proceedings of the 1st international conference on modeling and simulation of microsystems, semiconductors, sensors, and actuators (MSM'98), vol 1, Santa Clara, California, Marriot Computational Publications, pp 486–491
Beskok A, Karniadakis GE (1999) A model for flows in channels, pipes, and ducts at micro and nano scales. Microscale Therm Eng 3(1):43–77
Bestman AR, Ikonwa IO, Mbelegodu IU (1995) Transient slip flow. Int J Energ Res 19(3):275–277
Bhatnagar P, Gross E, Krook K (1954) A model for collision processes in gasses. Phys Rev 94:511–524
Bird GA (1978) Monte Carlo simulation of gas flows. Annu Rev Fluid Mech 10:11–31

Bird GA (1998) Molecular gas dynamics and the direct simulation of gas flows. Clarendon Press, Oxford

Caen R, Mas I, Colin S (1996) Ecoulements non permanents dans les microcanaux: réponse fréquentielle des microtubes pneumatiques. C R Acad Sci, Sér IIb 323:805–812

Cercignani C, Illner R, Pulvirenti M (1994) The mathematical theory of dilute gases, vol 106. Springer, Berlin Heidelberg New York

Chapman S, Cowling TG (1952) The mathematical theory of non-uniform gases. Cambridge University Press, Cambridge

Chen S, Doolen G (1998) Lattice Boltzmann method for fluid flows. Annu Rev Fluid Mech 30:329–364

Chen CS, Lee SM, Sheu JD (1998) Numerical analysis of gas flow in microchannels. Numer Heat Transf A 33:749–762

Colin S, Anduze M, Caen R (1998a) A pneumatic frequency generator for experimental analysis of unsteady microflows. In: Proceedings of the 1998 ASME International mechanical engineering congress and exposition, Anaheim, California, November 1998

Colin S, Aubert C, Caen R (1998b) Unsteady gaseous flows in rectangular microchannels: frequency response of one or two pneumatic lines connected in series. Euro J Mech B–Fluids 17(1):79–104

Colin S, Elizarova TG, Sheretov YV, Lengrand J-C, Camon H (2003) Micro-écoulements gazeux: validation expérimentale de modèles QHD et de Navier-Stokes avec conditions aux limites de glissement. In: CDROM de 16ème Congrès Français de Mécanique, Nice, France, September 2003

Colin S, Lalonde P, Caen R (2004) Validation of a second-order slip flow model in rectangular microchannels. Heat Transfer Eng 25(3):23–30

Deissler RG (1964) An analysis of second-order slip flow and temperature-jump boundary conditions for rarefied gases. Int J Heat Mass Transf 7:681–694

Ebert WA, Sparrow EM (1965) Slip flow in rectangular and annular ducts. J Basic Eng 87:1018–1024

Elizavora TG, Sheretov YV (2001) Theoretical and numerical investigation of quasi-gasdynamic and quasi-hydrodynamic equations. Comput Math Phys 41(2)219–234

Elizarova TG, Sheretov YV (2003) Analyse du problème de l'écoulement gazeux dans les microcanaux par les équations quasi hydrodynamiques. La Houille Blanche 5:66–72

Fan J, Shen C (1999) Statistical simulation of low-speed unidirectional flows in transition regime. In: Brun R, Campargue R, Gatigno Rl, Lengrand J-C (eds) Rarefied gas dynamics, vol 2. Cépaduès Editions, Toulouse, France, pp 245–252

Gad-el-Hak M (1999) The fluid mechanics of microdevices—the Freeman scholar lecture. J Fluid Eng 121:5–33

Grad H (1949) On the kinetic theory of rarefied gases. Commun Pure Appl Math 2:331–407

Harley JC, Huang Y, Bau HH, Zemel JN (1995) Gas flow in microchannels. J Fluid Mech 284:257–274

Hash D, Hassan H (1997) Two-dimensional coupling issues of hybrid DSMC/Navier-Stokes solvers. AIAA paper 97-2507:6333–6336

Hobson JP (1970) Accommodation pumping—a new principle for low pressure. J Vacuum Sci Technol 7(2):301–357

Hobson JP (1971) Analysis of accommodation pumps. J Vacuum Sci Technol 8(1):290–293

Hobson JP (1972) Physical factors influencing accommodation pumps. J Vacuum Sci Technol 9(1):252–256

Hudson ML, Bartel TJ (1999) DSMC simulation of thermal transpiration and accommodation pumps. In: Brun R, Campargue R, Gatigno Rl, Lengrand J-C (eds) Rarefied gas dynamics, vol 1. Cépaduès Editions, Toulouse, France, pp 719–726

Jie D, Diao X, Cheong KB, Yong LK (2000) Navier-Stokes simulations of gas flow in micro devices. J Micromech Microeng 10(3):372–379

Karniadakis GE, Beskok A (2002) Microflows: fundamentals and simulation. Springer, Berlin Heidelberg New York

Kennard EH (1938) Kinetic theory of gases, 1st ed. McGraw-Hill, New York

Lalonde P (2001) Etude expérimentale d'écoulements gazeux dans les microsystèmes à fluides. PhD thesis, Institut National des Sciences Appliquées, Toulouse, France

Lengrand J-C, Elizarova TG (2004) Microécoulements gazeux. In: Colin S (ed) Microfluidique, chapter 2. Hermès, Paris, France

Liu J, Tai Y-C, Ho C-M (1995) MEMS for pressure distribution studies of gaseous flows in microchannels. In: Proceedings of the 8th IEEE annual international workshop on micro-electro-mechanical systems (MEMS'95), an investigation of micro structures, sensors, actuators, machines, and systems, Amsterdam, The Netherlands, January/February 1995, pp 209–215

Loyalka SK, Hamoodi SA (1990) Poiseuille flow of a rarefied gas in a cylindrical tube: solution of linearized Boltzmann equation. Phys Fluids A 2(11): 2061–2065

Maurer J, Tabeling P, Joseph P, Willaime H (2003) Second-order slip laws in microchannels for helium and nitrogen. Phys Fluids 15(9):2613–2621

Mavriplis C, Ahn JC, Goulard R (1997) Heat transfer and flow-fields in short microchannels using direct simulation Monte Carlo. J Thermophys Heat Transf 11(4):489–496

Maxwell JC (1879) On stresses in rarefied gases arising from inequalities of temperature. Philos Trans R Soc 170:231–256

Mitsuya Y (1993) Modified Reynolds equation for ultra-thin film gas lubrication using 1.5-order slip-flow model and considering surface accommodation coefficient. J Tribol 115:289–294

Morini GL, Spiga M (1998) Slip flow in rectangular microtubes. Microscale Therm Eng 2(4):273–282

Muntz EP (1989) Rarefied gas dynamics. Annu Rev Fluid Mech 21:387–417

Muntz EP, Vargo SE (2002) Microscale vacuum pumps. In: Gad-el-Hak M (ed) The MEMS handbook. CRC Press, New York, pp 29.1–29.28

Norberg P, Ackelid U, Lundstrom I, Petersson LG (1997) On the transient gas flow through catalytically active micromachined channels. J Appl Phys 81(5):2094–2100

Oran ES, Oh CK, Cybyk BZ (1998) Direct simulation Monte Carlo: recent advances and applications. Annu Rev Fluid Mech 30:403–441

Pan LS, Liu GR, Lam KY (1999) Determination of slip coefficient for rarefied gas flows using direct simulation Monte Carlo. J Micromech Microeng 9(1):89–96

Pan LS, Ng TY, Xu D, Lam KY (2001) Molecular block model direct simulation Monte Carlo method for low velocity micro-gas flows. J Micromech Microeng 11(3):181–188

Piekos ES, Breuer KS (1996) Numerical modeling of micromechanical devices using the direct simulation Monte Carlo method. J Fluid Eng 118:464–469

Roveda R, Goldstein D, Varghese P (1998) Hybrid Euler/particle approach for continuum/rarefied flows. J Spacecraft Rockets 35(3):258–265

Sharipov F, Seleznev V (1998) Data on internal rarefied gas flows. J Phys Chem Ref Data 27(3):657–706

Shih JC, Ho C-M, Liu J, Tai Y-C (1996) Monatomic and polyatomic gas flow through uniform microchannels. ASME DSC 59:197–203

Sreekanth AK (1969) Slip flow through long circular tubes. In: Trilling L, Wachman HY (eds) Proceedings of the 6th international symposium on rarefied gas dynamics. Academic Press, New York, pp 667–680

Stefanov S, Cercignani C (1994) Monte Carlo simulation of a channel flow of a rarefied gas. Eur J Mech B–Fluids 13(1):93–114

Vargo SE, Muntz EP (1997) An evaluation of a multiple-stage micromechanical Knudsen compressor and vacuum pump. In: Proceedings of the 20th international symposium on rarefied gas dynamics (RGD-20). Beijing, China, pp 995–1000

Vargo SE, Muntz EP (1999) Comparison of experiment and prediction for transitional flow in a single-stage micromechanical Knudsen compressor. In: Brun R, Campargue R, Gatignol R, Lengrand J-C (eds) Rarefied gas dynamics, vol 1. Cépaduès Editions, Toulouse, France, pp 711–718

Vargo SE, Muntz EP, Shiflett GR, Tang WC (1999) Knudsen compressor as a micro- and macroscale vacuum pump without moving parts or fluids. J Vacuum Sci Technol A 17(4):2308–2313

Wu J-S, Tseng K-C (2001) Analysis of micro-scale gas flows with pressure boundaries using direct simulation Monte Carlo method. Comput Fluids 30(6):711–735

Xue H, Fan Q (2000) A new analytic solution of the Navier-Stokes equations for microchannel flow. Microscale Therm Eng 4(2):125–143

Young RM (1999) Analysis of a micromachine based vacuum pump on a chip actuated by the thermal transpiration effect. J Vacuum Sci Technol B 17(2):280–287